Design and fabrication of a hydroformed absorber for an evacuated flat plate solar collector

Applied Thermal Engineering 138 (2018) 456–464

Contents lists available at ScienceDirect

Applied Thermal Engineering

journal homepage: www.elsevier.com/locate/apthermeng

Design and fabrication of a hydroformed absorber for an evacuated flat plate solar collector

R.W. Moss[a,*], G.S.F. Shire[a], P. Henshall[b,1], P.C. Eames[c], F. Arya[d], T. Hyde[d]

[a] School of Engineering, University of Warwick, Coventry CV4 7AL, UK
[b] Oxford Institute for Sustainable Development, Oxford Brookes University, UK
[c] Centre for Renewable Energy Systems Technology, Loughborough University, UK
[d] School of the Built Environment, University of Ulster, UK

HIGHLIGHTS

- Flooded panel design overcomes poor thermal conductivity of stainless steel.
- Sufficiently uniform flow was achieved in each rectangular half-panel.
- 0.7 mm annealed stainless plate was required to withstand the 1 bar pressure load.
- Hydroforming trials at up to 48 MPa demonstrated the technique.
- 8 absorbers were built and pressure tested.

ARTICLE INFO

Keywords:
Solar collector
Evacuated
Vacuum
Hydroform
Flow distribution

ABSTRACT

The concept of an evacuated flat plate collector was proposed over 40 years ago but, despite its professed advantages, very few manufacturers have developed commercial versions. The absorber is a key component of a flat plate collector: in the context of an evacuated panel, absorber design poses a number of technical challenges.

A flooded panel absorber has been designed for use in evacuated flat plate solar collectors. The aim was to obtain higher efficiency, in a low out-gassing material, than would be possible using a conventional serpentine tube design.

Initial plans for a micro-channel plate were modified when optimisation analysis showed that a flooded panel could achieve as good performance with easier fabrication. The absorber plate is made from hydroformed stainless steel sheets welded together and features an array of through-holes for the glass-supporting pillars with the square panel subdivided into two rectangles connected in series for ease of fabrication and better flow distribution. The coolant flow was modelled in Star-CCM+. FEM simulations based on tensile test data informed the choice of sheet thickness and weld radius around the holes to withstand the 1 bar pressure differential.

Hydroforming is an effective method for producing sheet metal components, e.g. plates for heat exchangers or solar absorbers. As a thermal engineering experimental technique, the tooling is significantly cheaper than press tools since the mould does not need a matching die. In a research context, the ability to form plates in-house and explore profile and tooling options at low cost is very useful and might find application in other fields such as experimental heat exchangers.

A hydroforming facility was built using 85 mm thick steel sheet and a 25 MPa hydraulic pump. This proved highly effective at forming 0.7 mm stainless steel sheet. A total of eight absorbers were fabricated and successfully leak tested using helium. Two variants were made: one kind for use in enclosures with a metallic rear tray, the other for enclosures with glass on both sides. The collector efficiency factor is estimated to be 3% higher than for commercial tube-on-plate designs.

* Corresponding author.
E-mail address: r.moss@warwick.ac.uk (R.W. Moss).
[1] Formerly CREST, Loughborough University, UK.

https://doi.org/10.1016/j.applthermaleng.2018.04.033
Received 1 September 2017; Received in revised form 30 January 2018; Accepted 6 April 2018
Available online 13 April 2018

1. Introduction

1.1. Background

The concept of an evacuated flat plate (EFP) collector was proposed over 40 years ago but, despite its professed advantages, very few manufacturers have developed commercial versions. This situation suggests both technical difficulties in manufacturing a competitively-priced sealed for life panel and a lack of awareness of the benefits of such panels. Researchers at Warwick, Loughborough and Ulster universities have therefore developed and tested a number of evacuated flat plate collectors as part of an investigation into technical issues that might hinder manufacture and innovations that might improve efficiency. The dissemination of these results aims also to increase awareness of the efficiency benefits to end users.

One key component of a flat plate collector is the absorber plate: in the context of an evacuated panel, this poses a number of challenges. There is a compromise in the choice of material between thermal conductivity and risk of outgassing. The need for pillars or ribs to support the glass without any thermal conduction path from the plate also adds complexity.

Flat plate solar thermal collectors traditionally use a serpentine tube bonded or clipped to a conductive absorbing plate with a spectrally-selective black coating. Efficiency losses due to temperature variations across the plate can be minimised by using a high conductivity material such as copper and making it thick enough to give a high fin efficiency. A copper tube is typically soldered or laser welded to the back of the plate [1,2] to maximise the bond conductance.

Vacuum insulation has the potential to significantly reduce the heat loss coefficient U_L thereby allowing a collector to achieve satisfactory efficiency levels even when operating at “medium” temperatures of 100–200 °C for industrial process heat [3], under weak insolation or in cold environments [4]. An evacuated flat panel has higher optical efficiency than evacuated tubes.

A further requirement is that sufficient coolant flow can be achieved without an excessive pumping power requirement. Most installations use an electric circulating pump: an optimum pumping power [5], may be calculated from the cost ratio of heat to electricity and the system pressure drop. Micro-channel and flooded-panel absorbers can operate effectively with lower pumping powers than a serpentine design.

Commercial evacuated flat panels use a serpentine tube and plate design either with a copper sheet laser-welded to a stainless steel tube [6] or an aluminium sheet and copper tube [7]. The current project was intended to explore the potential of a micro-channel or similar novel architecture to create slim, architecturally attractive panels with high efficiency and low pressure drop. Many proprietary details of the SRB and TVP designs are undocumented: the theoretical and experimental investigation presented here is intended to provide definitive data to guide future evacuated flat plate collector designs. The fabrication technique may also find application in non-solar fields, for instance in the manufacture of experimental heat exchangers.

1.2. Choice of materials

Absorbers for vacuum-insulated enclosures [8] require materials with low outgassing rates in a vacuum [9]. Polymers are becoming a possibility for conventional solar collectors [10] but no currently available polymer has a sufficiently low outgas rate for use in an evacuated panel. Low-oxygen copper may be used [11]; solders containing high vapour pressure metals such as zinc should be avoided. Materials should also be able to withstand a bake-out at temperatures of 200 – 400 °C. Stainless sheet is commonly used for vacuum equipment [12,13] and can be vacuum baked [14] to reduce outgassing rates.

1.3. Absorber manufacturing technology and heat transfer modelling

Most commercial solar collectors use a serpentine tube configuration. This requires a plate to tube bond conductance > 30 W/m K [15]. Stainless steel has much lower thermal conductivity than copper or aluminium: careful design is then needed to minimise thermal resistance between plate and tube.

Mass produced panels usually use automated laser welding to join the plate and tube. Spyrou [16] has assessed stress development during welding and subsequent distortion. Laser welding copper sheet is difficult because the copper has very low absorption at typical laser wavelengths. Kuryntsev [17] and Moharana [18] overcame this problem, for butt welds, by focusing the laser onto the stainless steel and relying on conduction to melt the copper nearby.

Automated welding of a tube and plate absorber was not considered for this low volume research project on cost grounds.

Other joining technologies for solar absorbers include soft-soldering copper [19] and brazing [20,21]. Aluminium may be soldered to copper using specialist fluxes [22].

Thermal conductivity effects are greatly reduced if heat flow paths are shortened, for instance using a micro-channel or flooded panel design [5]. Kohole [23] investigated the effect of tube placement on efficiency and Tsilingiris [24] modelled the heat transfer implications of low-conductivity materials.

Hydroforming [25] is an effective technique for moulding thin sheets into shapes that would be suitable for a flooded panel. Prior experience of micro-channel plate manufacture at the University of Warwick together with the choice of stainless steel and manual welding led to the adoption of a hydroformed flooded panel design for the current project.

The purpose of this work was to investigate whether the thermal conductivity limitations of stainless steel could be overcome by a novel configuration which would also provide access for the cover glass support pillars. The design also avoided any combination of dissimilar metals in order to minimise thermal stresses and distortion. The target was to achieve a collector efficiency factor higher than commonly obtained from tube-on-plate designs. A secondary aim was to demonstrate that hydroforming could be used effectively in a research context to produce experimental apparatus. This was a novel and risky approach since there is very little published work in this area: distortion from residual stresses might have been too severe to allow welding into an assembly.

2. Experimental fabrication of a micro-channel plate

The initial concept for the evacuated collector was that it should use a micro-channel plate. This followed previous work at Warwick [26] and is attractive because the small hydraulic diameters lead to high heat transfer coefficients, thereby minimising the fluid-to-metal temperature difference. The collector efficiency factor $F'$is also high [5] due to the short conduction paths.

A pair of 200 mm × 140 mm absorbers were built [27]. This was a labour-intensive exercise and it became clear that the machining and manual welding time would be impracticable for a larger (0.5 × 0.5 m) panel. The time and cost could however be much reduced in a mass production context using a formed or extruded base plate with continuous, automated welding or using an alternative manufacturing technique, for instance roll-bonding [28,29]. For non-evacuated solar collectors, micro-channel absorbers could also be produced cheaply using injection-moulded polymers [30,31]: the low material conductivity necessitates a micro-channel or flooded design instead of a serpentine tube. Polymers were not considered for this project because they are currently unsuitable for high-vacuum, high-temperature use.

The stainless absorber proved to be well sealed, with water bath

checks using helium at 1 bar revealing just a couple of tiny leaks that were immediately repaired. The aluminium absorber however suffered from numerous weld leaks and it was infeasible to seal them all. Porosity in laser-welded aluminium is a complex topic [32]: it was not evident whether the leakage stemmed from micro-cracking or weld porosity. This clear difference between materials led to the choice of stainless steel instead of aluminium for all subsequent collectors.

Any design of collector (flooded, micro-channel or serpentine tube) will have an optimum channel size or plate-plate gap that balances the competing benefits of increased heat transfer coefficient and low thermal resistance at small hydraulic diameter and increased flow rate at large diameter [5].

Micro-channel and flooded designs provide a larger flow area and shorter passage length than a serpentine, at any given hydraulic diameter. The pumping power at a given flow rate is greatly reduced; conversely at a given pumping power a higher flow rate can be achieved. This minimises the fluid temperature rise and slightly improves the collector efficiency.

A detailed analysis of the optimum passage size [5] revealed that the optimum is a function of the intended system pumping power, plate length in the flow direction and fluid properties but is likely to be at least 1.6 mm. A flooded panel design is easier to manufacture than a microchannel plate and can achieve hydraulic diameters of this order without excessive sensitivity to welding distortion.

The choice of a flooded panel was subsequently confirmed by a design exercise for a stainless steel tube on plate absorber with a 10 mm diameter tube spot-welded to the plate at 30 mm intervals. A Bessel's equation radially symmetric approximation to the temperature field around each spot weld suggested that, even when using a 2 mm thick plate in an effort to overcome the low conductivity of stainless steel, the collector efficiency factor would have been only 0.933. The methodology will be described more fully in [33a].

3. Hydroforming trials

Stainless steel sheets in a mass production context can be quickly and easily formed by pressing; the costs of press tooling could not however be justified for a low-volume research project. Hydroforming offered an alternative using simpler tooling. The possibility of simple design modifications is an added advantage since a matching punch and die are not required.

The first trial used a pair of steel plates 125 × 100 × 12 mm that clamped a shim against an O-ring. The O-ring was made from stock material, cut to length and super-glued. The shim came from pack of stainless shims in 0.2, 0.25 and 0.3 mm thicknesses. The shape of the mould (Fig. 1(a)) was designed to test the shim's ability to deform into narrow channels, around corners and to leave "lands" that could be welded and provide space to the support pillar holes.

Initial testing showed that the shims easily tore when formed over corners. Rounding the corners improved the situation but the problem was ultimately identified by hardness measurements, HV = 434, which showed that the material was not in an annealed condition.

Some annealed shim stock was then procured with HV = 165. This did not tear, even with pressures as high as 48 MPa. The deformed shims closely followed the mould, even to the extent of showing embossed versions of the mould's end-mill machining marks. The hydraulic test pump was capable of higher pressures but at 48 MPa the O-ring started to extrude into the gap between the plates and needed replacing after a few tests. The plates themselves yielded slightly: the feed pipe and mould plates bowed in the centre by 0.14 and 0.06 mm respectively.

The basic equation for hydroforming assumes a 2-D cross-section with a constant-thickness sheet stretching to form an internal bend radius $r_{i,\min}$ that is effectively a section of a cylindrical pressure vessel.

$$r_{i,\min} = \frac{\sigma_y t}{p}$$

A typical $t = 0.3$ mm thick cross section after hydroforming at $p = 19.3$ MPa shows an internal bend radius of 6.5 mm, implying that the stress reached $\sigma = 418$ MPa. Tensile testing (Fig. 6, below) showed that annealed 316 stainless started to yield at $\sigma_y = 255$ MPa; the stress then rose above this level due to work hardening. Hydroforming theory is covered in more detail by Marciniak [34]. The hydroforming process for commercial components may involve highly detailed modelling [35].

Lower pressure tests gave a more rounded profile that was perfectly adequate for use in an absorber. This implied that a thicker sheet could be used with the pressures available.

4. Absorber design

4.1. Conceptual design

One attractive feature of a micro-channel design is that the manifolds can be designed to achieve uniform flow distribution over the surface. When using a flooded panel without manifolds there is less precise control over the internal flow, especially when the geometry is constrained by a uniform array of through-holes.

The simplest approach would be to take a square panel with inlet flow to one corner and outlet from the opposite corner. This is likely to result in flow running diagonally as it follows the shortest route: there would be stagnation regions in the two non-connected corners.

Considering the comparable problem of achieving uniform flow in a manifold and micro-channel system [36], the distribution becomes more uniform as the aspect ratio of passage length/manifold length increases. The increased pressure drop along channels reduces the

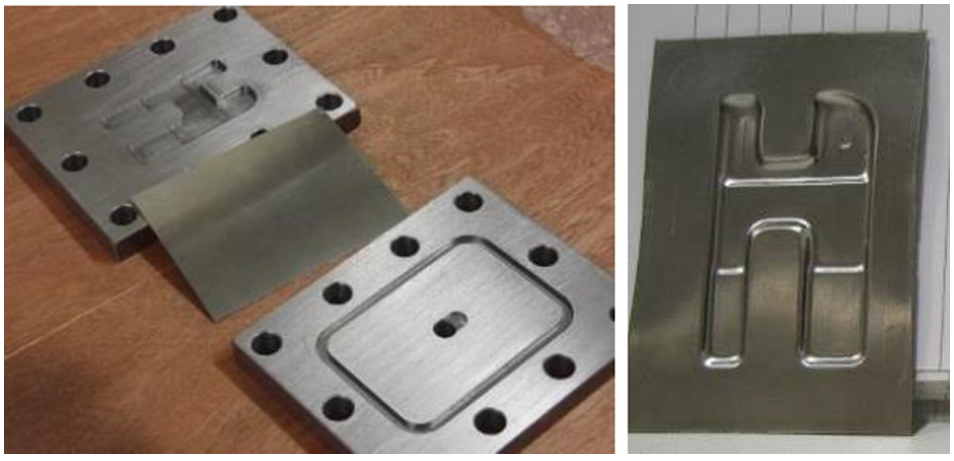

Fig. 1. (a) Mould and clamp plate for initial hydroforming trials, showing recesses of various depths and O-ring groove. (b) 0.2 mm sheet specimen formed at 34.5 MPa, seen from the pressurised side. The mould was designed to test features that would be necessary in an absorber such as concave and convex corners with variations in mould depth, width and corner radius.

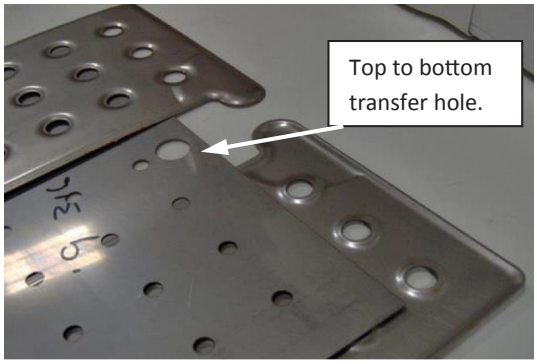

Fig. 2. Hydroformed and laser cut sheets prior to welding.

sensitivity to pressure differences in the manifolds. The flooded panel was therefore designed as two rectangular halves. The flow in each rectangle is still between opposite corners but for a given gap and flow rate the mean velocity will be higher.

This sub-division of the assembly meant that the absorber could be fabricated by welding two identical hydroformed sheets onto alternate sides of a flat base plate, Fig. 2, considerably reducing the size and weight of the hydroforming tools and minimising the risk of welding burn-through by avoiding butt welds between thin sheets.

Welding sheet metal commonly causes some distortion. The double-rectangle design with its 180° symmetry about a horizontal axis was expected to be slightly more stable and to distort less than a single hydroformed sheet covering one side of a flat base plate.

The enclosure size was limited to 0.5 × 0.5 m by vacuum oven capacity; with some allowance for the edge spacer and internal clearance, the absorber is 0.47 × 0.47 m.

The flooded panel concept, modelled as a pair of parallel plates, is the limiting case of a micro-channel analysis. Taking nominal design parameters of flow length $L = 1$ m (corner to corner over both panel halves), Tyfocor-LS at 70 °C and pumping power $W_p = 0.1$ W/m^2 leads to an optimum plate to plate gap of approximately 1.6 mm [5].

A further consideration was that the increased pressure drop from a narrower plate spacing would cause the flow to spread out with a more uniform distribution instead of taking the shortest possible route. A separation of less than 2 mm was deemed too risky since any distortion when welding might cause the plates to come together and touch. A 2 mm spacing was therefore chosen for the main section.

The flow near the flow and return pipes will be at a much higher velocity than at mid-panel because of the area contraction. This is likely to lead to increased head losses where the flow turns through 90° to leave or enter the tubes. The hydroformed plate is dished to provide a 3.5 mm gap in regions within 40 mm of the pipe ports to control the peak velocity.

4.2. Internal flow analysis

The flow was simulated in Star-CCM to check for low velocity or recirculating regions that might cause hot spots. The predicted flow distribution appears uniform across a mid-length horizontal plane in Fig. 3(a), without an obvious bias to one side or the centre. Towards the corners there is more variation but this is inevitable with a simple panel when using an array geometry without internal baffles and dividers to direct the flow. The 22 million node mesh was fine enough to resolve the plate-to-plate velocity distribution,Fig. 4.

Four of the eight sub-panel corners are stagnation regions. This cannot easily be avoided and the conduction path to regions of appreciable velocity was deemed short enough to avoid any risk of overheating. The final design used a 7 × 7 grid of support holes instead of the 11 × 11 shown in Fig. 3.

4.3. Collector efficiency factor

Duffie and Beckman [15] define the collector efficiency factor F' as the ratio of heat flux to fluid between the actual collector flux q_u' and the ideal collector equivalent with perfect thermal contact between fluid and absorber surface: $F' = \frac{q_u'}{G\tau\alpha - U_L(T_f - T_a)}$. F' may also be expressed as the ratio of two heat transfer coefficients: one from plate to environment, the other from fluid to environment: $F' = \frac{U_0}{U_L}$.

The collector efficiency factor for an absorber with a tube embedded in a plate is found [15] using:

$$F' = \frac{1/U_L}{W\left[\frac{1}{U_L[D+(W-D)F]} + \frac{1}{C_b} + \frac{1}{\pi D_h h_{fi}}\right]}$$

where $F = \frac{\tanh(m(W-D)/2)}{m(W-D)/2}, m = \sqrt{\frac{U_L}{k_m \delta}}$ with metal conductivity k_m and plate thickness δ. The more common situation where a tube is welded to one side of the plate may be modelled by setting $D = 0$. The efficiency factor is however overestimated in this case, unless thick-walled tube is used, because it takes no account of temperature variation around the tube as heat flows away from the contact point.

The upper surface of a flooded panel absorber may be modelled as a continuous sheet. Summing three thermal resistances in series (fluid to plate, conduction through the plate and heat loss to environment) leads to a simpler formula for this case:

$$F' = \frac{1/U_L}{\frac{1}{U_L} + \frac{d}{k} + \frac{1}{h_{fi}}}$$

Table 1 shows predicted efficiency factors for idealised absorbers with zero thermal resistance between tube and plate. The first case with 150 mm tube pitch is an estimate of the dimensions used in TVP's evacuated collector; the other cases take the 60 mm pillar pitch used in the present experiment. The efficiency factors for the tube on plate cases are over-estimates due to the assumption of infinite bond conductance and the neglect of any temperature distribution around the tube. This is particularly true when using stainless steel (second column). It was estimated (Section 2) that the bond resistance due to a series of spot welds at 30 mm intervals would reduce the efficiency factor to 0.933 in the stainless steel tube case.

The third column in Table 1 shows the expected performance of a flooded panel absorber. In this case there is no uncertainty regarding bond conductance because there is no tube and no bond line. At the nominal $U_L = 1$ W/m^2 K condition the efficiency factor is at least 3% higher than for the aluminium tube on plate result and 7% higher than expected in practice with a tube spot-welded to a stainless steel plate.

This conclusion is not limited to evacuated panels. The results at $U_L = 4$ W/m^2 K show that a flooded panel has a more significant efficiency advantage (0.993 versus 0.888) when subjected to the higher heat loss coefficients in a conventional flat plate collector.

4.4. Design to withstand operational stresses

The material must be sufficiently thick and strong enough to withstand the ⩾ 1 bar pressure difference in an evacuated enclosure without rupture or excessive distortion. There were two areas of particular interest: the central deflection in the flat regions between each group of four holes and the stresses in and around the weld zones.

Each stainless steel sheet was modelled as a "shell" in Abaqus CAE™ to avoid the need for a 3D grid with closely-spaced nodes in the through-sheet direction. Deflections and stresses were analysed both for an axisymmetric model of the region around a single hole and for a nominal rectangular panel.

The Abaqus sheet model was drawn assuming that the hydroformed sheet would locally adopt a toroidal profile, Fig. 5, as it stretched to its elastic limit over each circular island on the former.

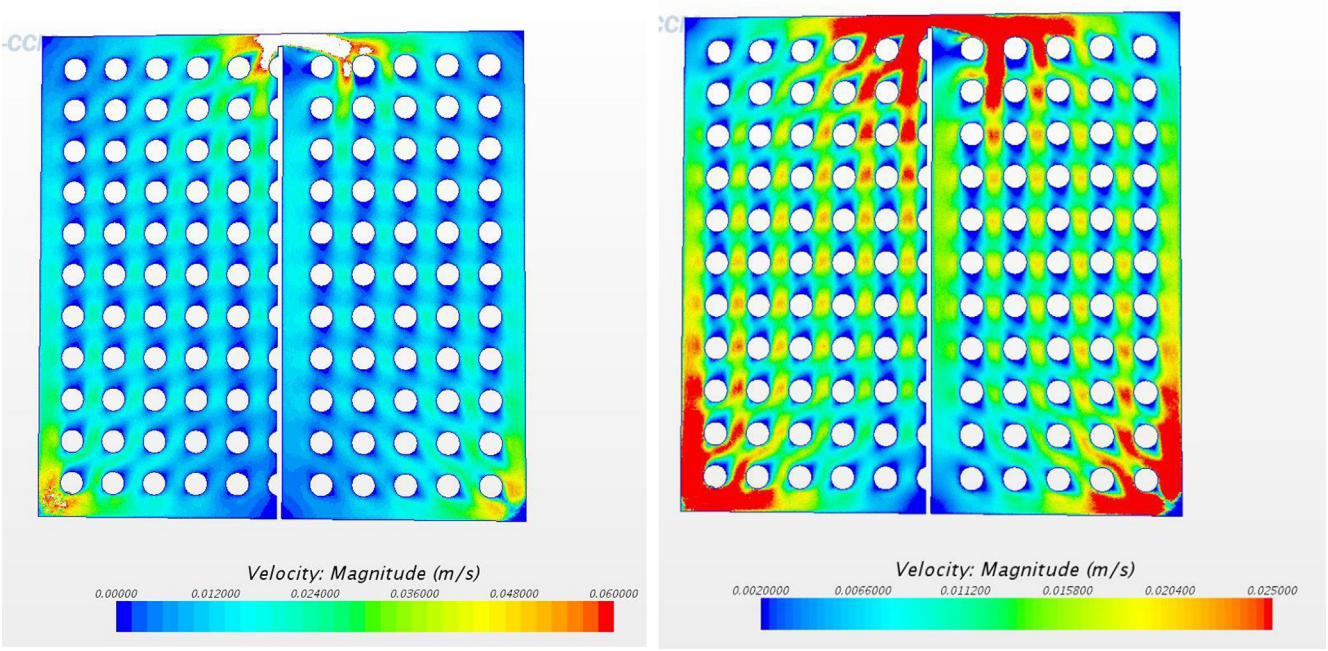

Fig. 3. Predicted water speed (Star-CCM, 22 million nodes). (a) Flow is from left to right and there is evidence of a "jet" from the transfer port in the left-hand image (scale 0 → 0.06 m/s).

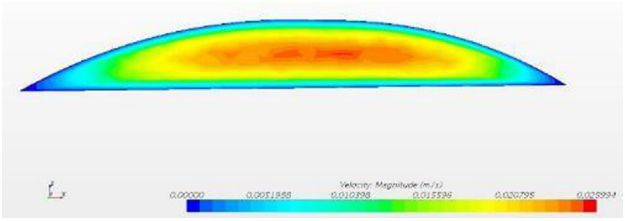

Fig. 4. View of a typical cross-section between two holes. [Scale 0 → 0.026 m/s].

Table 1
Assumed parameters and collector efficiency factors for tube on plate and flooded panel absorbers using Tyfocor-LS® at 60 °C, laminar flow. 4 W/m^2 K would be a typical U_L heat loss coefficient for a non-evacuated flat plate whereas 1 and 0.4 represent nominal and highest feasible coefficients for an evacuated collector.

Type	Tube on plate	Tube on plate	Flooded panel
Sheet material	Aluminium	304L stainless steel	316L stainless steel
Sheet thickness	1 mm	1.6 mm	0.8 mm
Hydraulic diameter	12 mm	12 mm	4 mm
Tube internal, external diameter	12, 14 mm	12, 14 mm	2 mm gap
Tube pitch	150 mm	60 mm	n/a
Bond conductance	∞	∞	n/a
F' (U_L = 4 W/m^2 K)	0.881	0.921	0.993
F' (U_L = 1 W/m^2 K)	0.967	0.979	0.9983
F' (U_L = 0.4 W/m^2 K)	0.987	0.991	0.9993

Two hydroformed profiles were studied. The toroidal areas around each hole blend into a pattern of flat regions surrounded by 4 holes: increasing the size of the toroid reduces the flat area and means that a larger proportion of the plate is stiffened by the 3D nature of the toroidal curve. The island diameter is the same in each case since the difference between the two models can be achieved by altering the hydroforming pressure.

The material chosen was T316 sheet in 2B annealed state. A tensile test specimen was cut from sheet and tested to determine its stress/strain characteristics, Fig. 6. These were converted to true stress and true strain as required in Abaqus.

A 3 × 3 pattern of support holes was used for the rectangular panel FE analysis instead of the full 3 × 7 in each side-panel (Fig. 7, 0.8 mm sheet top and bottom, "wider" toroids); this simplified the manual input requirements when meshing. After a number of simulations with various thicknesses and weld ring diameters a sheet thickness of 0.7 mm (hydroformed), 0.9 mm (baseplate) was chosen. One important feature is that the weld ring diameter (20 mm) is larger than the hole diameter (13 mm): this reduces stress levels in and around the weld.

The final design increased thickness from 0.6 to 0.7 mm to limit the peak stress in the vicinity of the weld. To avoid tearing, the hydroformed sheet has a blend radius around the lip of the moulding island. The weld line in the Abaqus model (arrowed) is therefore offset inwards from the apparent intersection. The lip here is also necessary to allow clamping while welding and to reduce the risk of burn through.

The choice of 0.7 mm sheet was a compromise between operational stresses and ease of hydroforming. The base plate did not require hydroforming and could in principle use much thicker material to minimise the risk of distortion: the flat sheet does not have any toroidal surfaces to stiffen it. A 0.9 mm base was chosen because welding is easier if the sheets are not too dissimilar in thickness. The von Mises peak stress of approximately 480 MPa at a differential pressure ΔP = 2 bar, Fig. 7(a), is for a worst case e.g. during leak testing. When operating with coolant at ambient pressure in an unpressurised circuit the peak stress would be of order 240 MPa and hence less than the initial yield stress. The highly ductile nature of the stainless steel allows the possibility of stress relief via slight deformation in the high stress regions without risk of failure.

5. Design of the hydroforming facility

The hydroforming clamp plates and mould plate (Fig. 8) were machined from S355 high-yield structural steel. A thickness of 85 mm was chosen for the clamp plates based on a rectangular slab stress formula for a uniformly loaded rectangular plate of length a and width b [37]:

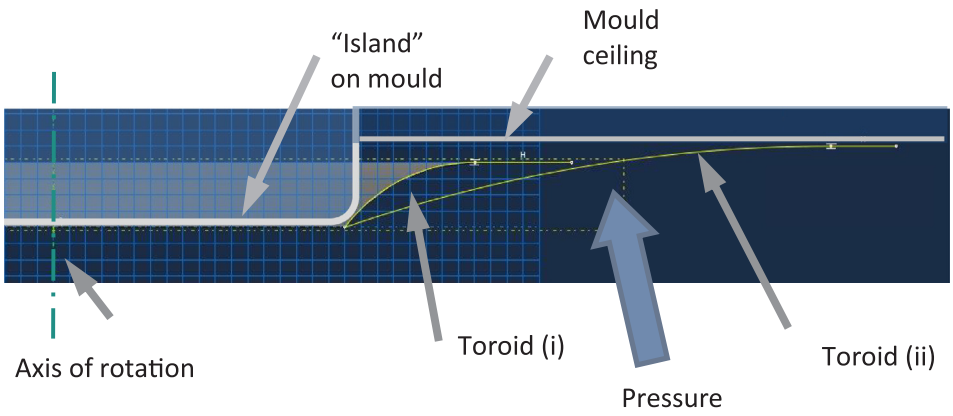

Fig. 5. Cross-section of toroidal profiles as modelled in Abaqus. The mould line for toroid (ii) is included here simply to illustrate how the shape is generated: the Abaqus simulations described below are for a free (unenclosed) panel.

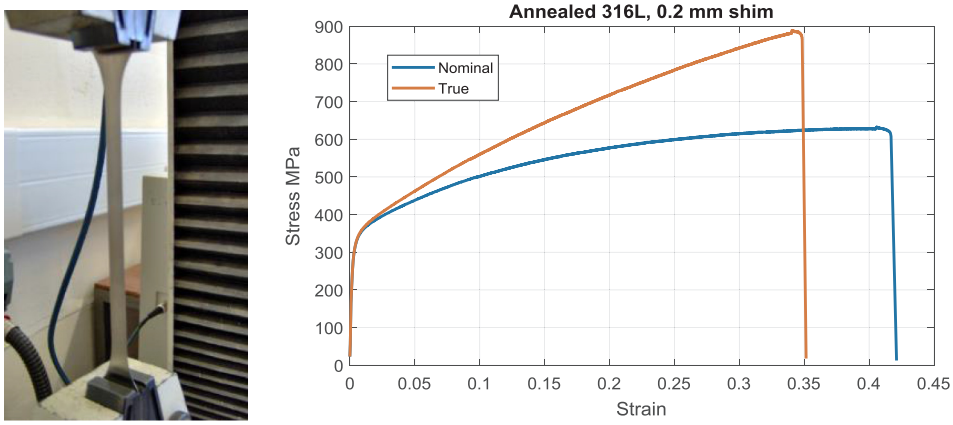

Fig. 6. (a) Tensile test of T316 specimen, (b) nominal and true stress/strain characteristics. The specimen started to yield at 255 MPa and failed at a nominal strain of 42%.

$\sigma_{max} = \frac{\beta p b^2}{t^2}$ using $\beta = 0.557$ for $\frac{a}{b} = 1.75$.

This models the pressure-loaded area only and the stress may be an over-estimate for a larger plate loaded only over a central region.

The formula gives a peak stress approximately 26% lower than obtained for an infinitely long plate. The yield stress of 355 MPa would be achieved at a hydraulic pressure of 57.4 MPa, implying a safety factor of 2.3 at the design pressure of 25 MPa.

Grade 8.8 M27 bolts tightened to 600 N m with greased threads and washers clamp the stainless sheet between the mould and lower clamp plates. The sheet is pushed against an O-ring that sits in a groove in the clamp plate. The torque is less than the recommended tightening torque (≈1390 N m) but was the highest that could easily be achieved with the available torque wrench. An online torque calculator [38] suggests that 600 N m creates a preload of approximately 131 kN in each bolt.

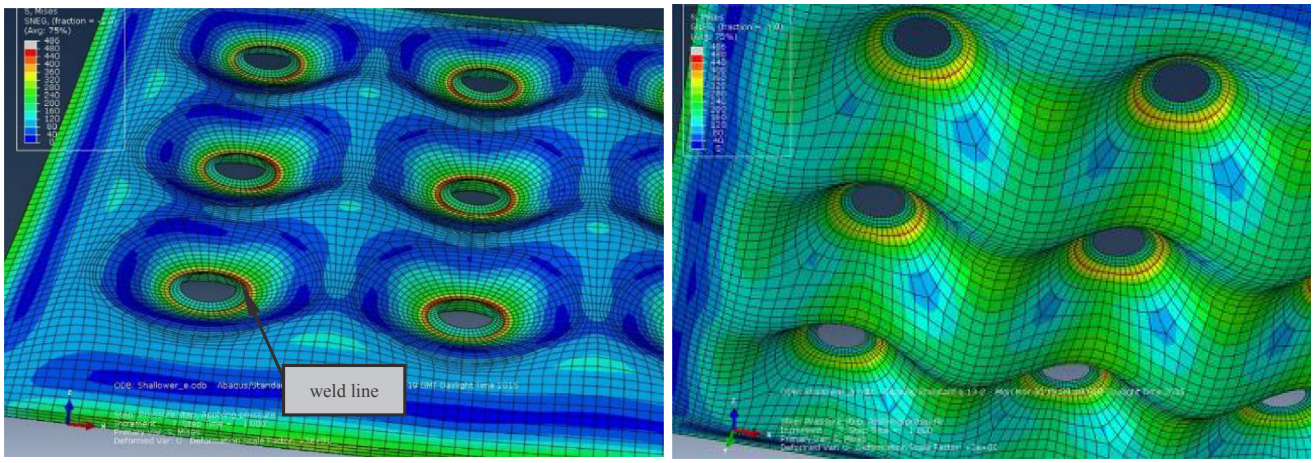

Fig. 7. Abaqus simulation of deflections (exaggerated here) and von Mises stresses in the hydroformed plate (left) and base plate (right) for 0.8 mm sheet at $\Delta P = 2$ bar. The colour bar runs from 0 to 486 MPa in each case.

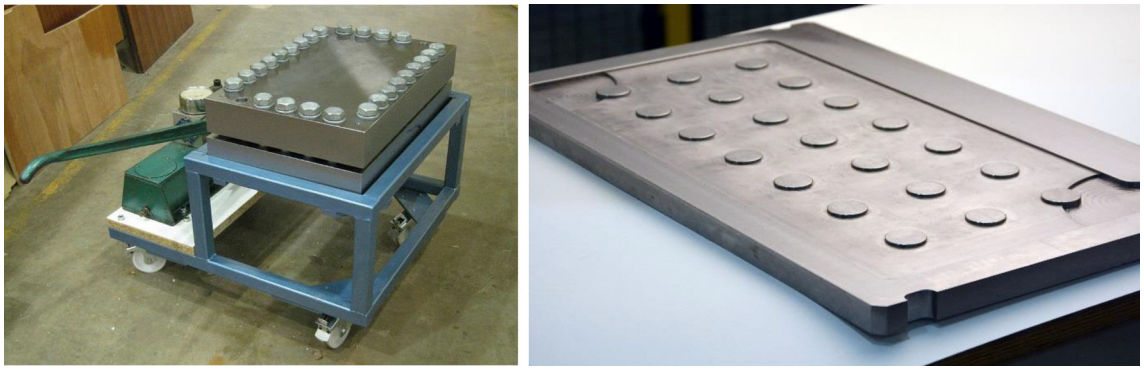

Fig. 8. (a) The hydroforming facility, (b) the mould plate. The surface seen here faces downwards in the facility.

The bolt line load in the centre of a long side may be calculated as:

$R = \gamma p b$ [37] using $\gamma = 0.497$ at this aspect ratio.

At 25 MPa the load in the side bolts (56 mm pitch) would be 194 kN and the bolts would stretch elastically by 0.10 mm relative to the pre-loaded length. There was some evidence of leakage past the O-ring seal at this condition which might indicate that the plates were starting to separate slightly. This was not a significant problem and could perhaps have been overcome by tightening to a higher torque. A total of 19 sheets were hydroformed.

Oil is fed underneath the 0.7 mm sheet and pushes it up against a 20 mm thick mould plate, Fig. 8(b), that is held between the two clamp plates. The mould plate is NC-milled, leaving 21 “islands” to form the depressions in the sheet for the support holes and their circular welds. An overhead crane with a magnetic chuck was used to aid removal of the 180 kg clamp plates.

6. Absorber fabrication

6.1. Welding the hydroformed panels

Two competing enclosure designs were developed for the evacuated collector project [8], Fig. 9. These required two different feed tube arrangements.

- The first design used a stainless steel tray covered by a single glass sheet and has absorber feed tubes pointing downwards through the back of the tray.
- The second design used a symmetrical pair of glass panes held apart by a stainless steel edge spacer. This is intended for use in building facades where its attractive appearance from both inside and outside would be an advantage. The feed tubes are in line with the absorber and pass through the edge seal. A pair of cylindrical manifolds distribute or collect the pipe flow over 4 cm of the absorber edge and simplify the welding of the tube/absorber junction.

The hydroformed sheets were manually TIG welded. Each absorber was then water-bath tested for leaks using helium at 1.4 bar.

6.2. Distortion testing

Measurements of thickness and any distortion due to variations in pressure were required to determine the minimum safe height within the evacuated enclosure. An absorber was supported at 3 points on a surface table, Fig. 10, and the surface height was measured at 13 points both unpressurised and at 1 bar gauge. Measurements were taken with the absorber both front-side up and upside down. The maximum displacement due to an applied 1 bar pressure was < 1 mm.

6.3. Installation and testing

The process of assembling the vacuum enclosures will be described in a forthcoming pair of papers by Arya [33a,b]. The chrome plating, testing and experimental results are presented in [39].

7. Conclusions

A number of absorber concepts were investigated. A flooded panel absorber made from hydroformed plates was adopted because it offered higher efficiency than a serpentine tube arrangement and was easier to manufacture than a micro-channel architecture. Previous experience

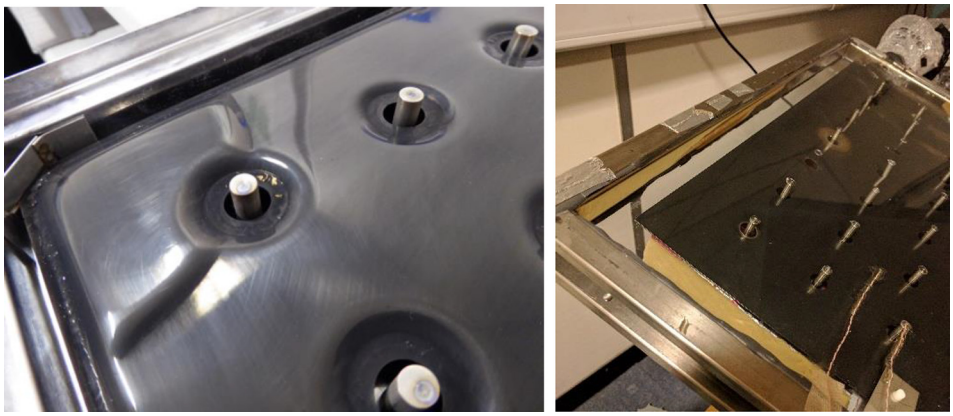

Fig. 9. (a) Tray-type collector prior to adding the cover glass. Using a stainless steel tray allows the pins to be spot-welded in place. The absorber has been black chrome plated. (b) Completed “symmetrical” enclosure.

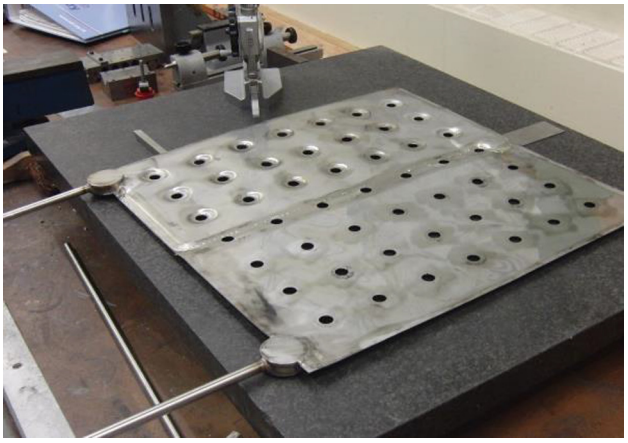

Fig. 10. A symmetrical absorber undergoing distortion measurements. The cylindrical stub manifolds are visible on the left-hand side.

fabricating microchannel absorbers in aluminium and stainless steel led to the choice of stainless steel as a suitable vacuum-compatible material despite its relatively low thermal conductivity.

CFD simulations showed that an effective flow distribution could be obtained by sub-dividing the absorber into two rectangular halves, each with flow entering and leaving at opposite corners. The collector efficiency factor is predicted to be 3% higher than for a typical aluminium tube-on-plate design and 7% higher than would have been possible using a spot-welded stainless steel plate.

FE analysis based on tensile test material properties proved that a material thickness of 0.7 mm was sufficient to withstand operational pressures. The peak stress is approximately 240 MPa when subject to a 1 bar pressure differential.

Hydroforming proved to be an effective technique for forming sheet metal in a research context. Pressures of 25 MPa were found to work well in deforming a 0.7 mm stainless sheet. The hydroforming rig concept, with sheet metal sealed against an O-ring, was successfully demonstrated. Pressure testing showed that a 1 bar pressure differential (representative of operation in a vacuum enclosure) distorted the completed absorbers by less than 1 mm.

The flooded panel solar absorber concept could be easily adapted for mass production using high speed press tools and automated welding. For small volume production, hydroforming is a useful workshop technique and could be useful for experimental heat exchanger components as well as solar absorbers. The flow and stress predictions presented here may provide useful insights for other fields such as radiators and blow-moulded components.

Acknowledgements

The authors are grateful to the Engineering and Physical Sciences Research Council (EPSRC) for funding this work as part of a collaborative programme between Warwick, Loughborough and Ulster universities, reference EP/K009915/1, EP/K010107/1 and EP/K009230/1. Data and images used in this paper are openly available from http://wrap.warwick.ac.uk/id/eprint/89676.

References

[1] U. Duerr, Welding thermal solar absorbers, Ind. Laser Solut. 21 (9) (2006) 12–14.
[2] C. Rüttimann, U. Dürr, A Moalem, M. Priehs, Reliable laser micro-welding of copper, in: Proc. SPIE 7920, Laser Applications in Microelectronic and Optoelectronic Manufacturing (LAMOM) XVI, 792007 (February 21, 2011). < http://spie.org/Publications/Proceedings/Paper/10.1117/12.875033 > (downloaded 30/1/2018).
[3] ETSAP, Solar Heat for Industrial Processes (IEA-ETSAP and IRENA Technology Brief E21), 2015. < http://www.irena.org/DocumentDownloads/Publications/IRENA_ETSAP_Tech_Brief_E21_Solar_Heat_Industrial_2015.pdf > (downloaded 30/1/2018).
[4] R.W. Moss, P. Henshall, F. Arya, G.S.F. Shire, T. Hyde, P.C. Eames, Performance and operational effectiveness of evacuated flat plate solar collectors compared with conventional thermal, PVT and PV panels.
[5] R.W. Moss, G.S.F. Shire, P. Henshall, P.C. Eames, F. Arya, T. Hyde, Optimal passage size for solar collector micro-channel and tube-on-plate absorbers, Sol. Energy 153 (September) (2017) 718–731, http://dx.doi.org/10.1016/j.solener.2017.05.030.
[6] C. Benvenuti, V. Ruzinov, The SRB evacuated flat solar panel, in: Proceedings of ECOS, 2010, pp. 429–434. < http://infoscience.epfl.ch/record/165003/files/Ecos2010-book2-printing.pdf?version=5 > (downloaded 30/1/2018).
[7] TVP Solar, MT-30 datasheet. < http://www.tvpsolar.com/files/pagine/1508933997_MT-PowerDatasheet (v4 SK).pdf > (downloaded 30/1/2018).
[8] P. Henshall, P. Eames, F. Arya, T. Hyde, R. Moss, S. Shire, Constant temperature induced stresses in evacuated enclosures for high performance flat plate solar thermal collectors, Sol. Energy 127 (2016) 250–261.
[9] S. Sgobba, Materials for high vacuum technology: an overview, CERN, 2006. < https://cds.cern.ch/record/983744/files/p117.pdf > (downloaded 30/1/18).
[10] A. Klein, G. Oreski, K. Resch-Fauster, Applicability of technical biopolymers as absorber materials in solar thermal collectors, Sol. Energy 153 (2017) 276–288.
[11] Y. Koyatsu, H. Miki, F. Watanabe, Measurements of outgassing rate from copper and copper alloy chambers, Vacuum 47 (6–8) (1996) 709–711.
[12] J.-P. Bacher, C. Benvenuti, P. Chiggiato, M.-P. Reinert, S. Sgobba, A.-M. Brass, Thermal desorption study of selected austenitic stainless steels, J. Vac. Sci. Technol., A 21 (2003) 167, http://dx.doi.org/10.1116/1.1527953.
[13] D. Coyne, LIGO vacuum compatible materials list (LIGO project internal working note) April 2004. < https://dcc.ligo.org/LIGO-E960050/public > (downloaded 30/1/18).
[14] M. Leisch, Hydrogen outgassing of stainless steel our present knowledge, in: 1st Vacuum Symposium, February 2010. < www.vacuum-uk.org/pdfs/vs1/vs1/Leisch.pdf > (downloaded 30/1/18).
[15] J.A. Duffie, A. Beckman, Solar Engineering of Thermal Processes, Wiley, 2013.
[16] L.A. Spyrou, N. Aravas, Thermomechanical modelling of laser spot welded solar absorbers, ASME J. Manuf. Sci. Eng., 137 (February) (2015) 011016-1:15.
[17] S.V. Kuryntsev, A.E. Morushkin, A.Kh. Gilmutdinov, Fiber laser welding of austenitic steel and commercially pure copper butt joint, Opt. Lasers Eng. 90 (2017) 101–109.
[18] B.R. Moharana, S.K. Sahu, S.K. Sahoo, R. Bathe, Experimental investigation on mechanical and microstructural properties of AISI 304 to Cu joints by CO_2 laser, Eng. Sci. Technol. Int. J. 19 (2016) 684–690 <https://www.sciencedirect.com/science/article/pii/S2215098615001652>.
[19] A. Klimpel, J. Górka, A. Czupryński, T. Kik, R. Dadak, Research into GTA automatic soft soldering technology for solar energy collector components, Weld. Int. 26 (2) (2012) 112–117 <http://www.tandfonline.com/doi/full/10.1080/09507116.2010.540854> (downloaded 11/8/2017).
[20] A. Klimpel, T. Kruczek, A. Lisiecki, D. Janicki, Experimental analysis of heat conditions of the laser braze welding process of copper foil absorber tube for solar collector elements, Weld. Int. 27 (6) (2013) 434–440 <http://www.tandfonline.com/doi/full/10.1080/09507116.2011.606140> (downloaded 11/8/2017).
[21] V.M. Rybaulin, A.V. Skorobatyuk, A.V. Mikitas, Brazing of absorbers of planar solar heating collectors produced from materials of the Cu–CuZn system, Weld. Int. 30 (2) (2016) 142–149 <http://www.tandfonline.com/doi/full/10.1080/09507116.2015.1036534> (downloaded 11/8/2017).
[22] Z. Mirski, K. Granat, H. Drzeniek, T. Piwowarczyk, T. Wojdat, Soldering of aluminium with copper, Weld. Int. 27 (3) (2013) 190–195 <http://www.tandfonline.com/doi/full/10.1080/09507116.2011.600029> (downloaded 11/8/2017).
[23] Y.W. Koholé, G. Tchuen, Comparative study of three thermosyphon solar water heaters made of flat-plate collectors with different absorber configurations, Int. J. Sustain. Energy 36 (5) (2017) 430–449 <http://www.tandfonline.com/doi/abs/10.1080/14786451.2015.1035272?journalCode=gsol20> (downloaded 11/8/2017).
[24] P.T. Tsilingiris, Heat transfer analysis of low thermal conductivity solar energy absorbers, Appl. Therm. Eng. 20 (2000) 1297–1314.
[25] M. Koç, S. Mahabunphachai, E. Billur, Forming characteristics of austenitic stainless steel sheet alloys under warm hydroforming conditions, Int. J. Adv. Manuf. Technol. (2011), <https://link.springer.com/article/10.1007/s00170-011-3169-x> (downloaded 11/8/2017).
[26] M.A. Oyinlola, G.S.F. Shire, R.W. Moss, The significance of scaling effects in a solar absorber plate with micro-channels, Appl. Therm. Eng. 90 (2015) 499–508.
[27] R.W. Moss, G.S.F. Shire, Design and performance of evacuated solar collector microchannel plates. In: Conference Proceedings: EuroSun 2014, Aix-les-Bains (France), 16–19 September 2014, http://proceedings.ises.org/paper/eurosun2014/eurosun2014-0039-Moss.pdf.
[28] M. Hermann, Development of a bionic solar collector with aluminium roll-bond absorber, BIONICOL Final Report. <http://www.bionicol.eu/> (downloaded 18/6/2014).
[29] X. Sun, J. Wu, Y. Dai, R. Wang, Experimental study on roll-bond collector/evaporator with optimized channel used in direct expansion solar assisted heat pump water heating system, Appl. Therm. Eng. 66 (2014) 571–579.
[30] M. Do Ango, M. Medale, C. Abid, Optimization of the design of a polymer flat plate solar collector, Sol. Energy 87 (2013) 64–75.
[31] S. Kim, J. Kissick, S. Spence, C. Boyle, Design, analysis and performance of a polymer–carbon nanotubes based economic solar collector, Sol. Energy 134 (2016) 251–263.
[32] G. Verhaege, Achieving aerospace-standard porosity levels when welding thin and thick section aluminium using fibre-delivered lasers, [EngD Thesis] Springer, 2008.
[33] F. Arya, R.W. Moss, T. Hyde, S. Shire, P. Henshall, P.C. Eames, Vacuum enclosures

for solar thermal panels Part 1: fabrication and hot-box testing; Part 2: transient testing with an uncooled absorber plate (forthcoming).
[34] Z. Marciniak, J.L. Duncan, S.J. Hu, Mechanics of Sheet Metal Forming, second ed., Butterworth-Heinemann, Chapter 11 (Hydroforming), 2002, ISBN 0 7506 5300 0.
[35] L.-P. Lei, Jeong Kim, S.-J. Kang, B.-S. Kang, Rigid–plastic finite element analysis of hydroforming process and its applications, J. Mater. Process. Technol. 139 (2003) 187–194. < https://www.sciencedirect.com/science/article/pii/S0924013603002188 > .
[36] D. Tondeur, Y. Fan, J.-M. Commenge, L. Luo, Uniform flows in rectangular lattice networks, Chem. Eng. Sci. 66 (2011) 5301–5312.
[37] W.C. Young, R.G. Budynas, Roark's Formulas for Stress and Strain, seventh ed., McGraw-Hill, 2002.
[38] Stanley torque calculator. < http://www.stanleyengineeredfastening.com/brands/spiralock/information-center/torque-calculator > (downloaded 9/6/17).
[39] R.W. Moss, P. Henshall, F. Arya, G.S.F. Shire, P.C. Eames, T. Hyde, Simulator testing of evacuated flat plate solar collectors for industrial heat and building integration, Sol. Energy 164 (April) (2018) 109–118, http://dx.doi.org/10.1016/j.solener.2018.02.004.